Journal of Neural Engineering

PAPER

Ultra-high-resolution time-frequency analysis of EEG to characterise brain functional connectivity with the application in Alzheimer's disease

Jun Cao[1], **Yifan Zhao**[1,*], **Xiaocai Shan**[1,2], **Daniel Blackburn**[3], **Jize Wei**[4], **John Ahmet Erkoyuncu**[1], **Liangyu Chen**[5] and **Ptolemaios G Sarrigiannis**[6]

[1] School of Aerospace, Transport and Manufacturing, Cranfield University, Cranfield, United Kingdom
[2] Institute of Geology and Geophysics, Chinese Academy of Sciences, Beijing 100029, People's Republic of China
[3] Department of Neurosciences, Sheffield Teaching Hospitals, NHS Foundation Trust, Royal Hallamshire Hospital, Sheffield, United Kingdom
[4] Department of Applied Mathematics, The Hong Kong Polytechnic University, Hong Kong, People's Republic of China
[5] Department of Neurosurgery, Shengjing Hospital of China Medical University, Shenyang, People's Republic of China
[6] Royal Devon and Exeter NHS Foundation Trust, Exeter EX2 5DW, United Kingdom
[*] Author to whom any correspondence should be addressed.

E-mail: yifan.zhao@cranfield.ac.uk

Keywords: electroencephalogram (EEG), revised Hilbert–Huang transformation (RHHT), peak frequency of cross-spectrum (PFoCS), support vector machine (SVM), topographic visualisation

Supplementary material for this article is available online

OPEN ACCESS

RECEIVED
28 December 2021

REVISED
19 July 2022

ACCEPTED FOR PUBLICATION
27 July 2022

PUBLISHED
11 August 2022

Abstract

Objective. This study aims to explore the potential of high-resolution brain functional connectivity based on electroencephalogram, a non-invasive low-cost technique, to be translated into a long-overdue biomarker and a diagnostic method for Alzheimer's disease (AD). *Approach.* The paper proposes a novel ultra-high-resolution time-frequency nonlinear cross-spectrum method to construct a promising biomarker of AD pathophysiology. Specifically, using the peak frequency estimated from a revised Hilbert–Huang transformation (RHHT) cross-spectrum as a biomarker, the support vector machine classifier is used to distinguish AD from healthy controls (HCs). *Main results.* With the combinations of the proposed biomarker and machine learning, we achieved a promising accuracy of 89%. The proposed method performs better than the wavelet cross-spectrum and other functional connectivity measures in the temporal or frequency domain, particularly in the Full, Delta and Alpha bands. Besides, a novel visualisation approach developed from topography is introduced to represent the brain functional connectivity, with which the difference between AD and HCs can be clearly displayed. The interconnections between posterior and other brain regions are obviously affected in AD. *Significance.* Those findings imply that the proposed RHHT approach could better track dynamic and nonlinear functional connectivity information, paving the way for the development of a novel diagnostic approach.

1. Introduction

Alzheimer's disease (AD) is one of the most common neurodegenerative diseases, resulting in the loss of memory and other cognitive impairments (Ferreri *et al* 2016, Blinowska *et al* 2017). The number of patients affected by AD and the difficulties in treating this disorder provoke massive demands for the early diagnosis of the condition and effective approaches for monitoring disease progression. In the past decades, electroencephalogram (EEG) has attracted significant interest since it is economical, non-invasive and with an ultra-high time resolution. A variety of biomarkers were extracted from EEGs in AD-related research, such as amplitude (Poil *et al* 2013), power spectral densities (PSDs) (Wang *et al* 2015b, Liu *et al* 2016), phase-related features (Engels *et al* 2015, Kent *et al* 2021), alpha rhythm power (Babiloni *et al* 2013, Schmidt *et al* 2013, Sadaghiani and Kleinschmidt 2016, Benwell *et al* 2020) wavelet

energy (Jeong *et al* 2016), features from graph theory (Miraglia *et al* 2016, delEtoile and Adeli 2017) and brain connectivity estimations (Blinowska *et al* 2017, delEtoile and Adeli 2017, Vecchio *et al* 2017, Yu *et al* 2018, Durongbhan *et al* 2019, Zhao *et al* 2020). Peak frequency is also a promising biomarker in the field of dementia and other neurodegenerative disorders (Grandy *et al* 2013). To support the classification of AD based on those features extracted from EEG recordings, many machine learning algorithms have been employed, such as linear discriminant analysis, logistic regression, random forest, support vector machines (SVMs), K-nearest neighbour (KNN) and deep learning (Qiao *et al* 2018, Durongbhan *et al* 2019, Vecchio *et al* 2020, Gunawardena *et al* 2021).

Alpha and Beta peak frequency of a single channel was used as a quantitative EEG (qEEG) measure for the classification between AD and mild cognitive impairment (MCI). MCI represents a transitional period of neurological degeneration from normal ageing to AD (Poil *et al* 2013). That is to say, the peak frequency may be a potential biomarker to evaluate the degree of brain degeneration. Dementia with Lewy bodies can also be discriminated from AD since it has a significantly lower peak frequency (van der Zande *et al* 2018). However, Idaji *et al* (2022) suggested that the peak frequency in the Beta band may be a harmonic activity from the Alpha band and this observation requires further investigation. Besides, different from young adults, older people show significant slowing of individual alpha peak frequency. In a word, there is increasing evidence from the literature suggesting the EEG peak frequency has great potential to advance dementia research and possibly one day be translated into a clinically useful AD diagnostic tool.

However, most of the previous related techniques are univariate-based methods. That is to say, those techniques are trying to obtain independent features from each EEG channel. However, there is evidence suggesting brain disorders affect information exchange between multiple brain areas, namely brain connectivity (Varotto *et al* 2014, McBride *et al* 2015, Hassan *et al* 2017, Cao *et al* 2021a). To be more specific, brain connectivity is divided into three well-accepted categories: neuroanatomical brain connectivity, functional brain connectivity, and effective brain connectivity (Abbasvandi and Nasrabadi 2019, Cao *et al* 2021b). Neuroanatomical connectivity refers to structural links such as synapses or fibre pathways at the microscopic scale of neurons (Cao *et al* 2021b). In terms of effective connectivity, it indicates the directed causal influence of one neural region over others. On the other hand, functional brain connectivity is defined as the statistical strength of covariance and/or correlation between pairs of brain regions, typically estimated with correlation, coherence, and information theory (Mheich *et al* 2015, Allen 2018). Many researchers demonstrated that brain connectivity is able to reflect complex cortical interconnections among brain networks and the state of independent brain regions (Sakkalis 2011, van Mierlo *et al* 2014, Durongbhan *et al* 2019, Tafreshi *et al* 2019). Furthermore, it can reveal distinct aspects characterising various neurological conditions, such as dementia and other neurodegenerative diseases. There is evidence that both anatomical and functional connections among neural areas are affected in various forms of neurodegeneration (Pijnenburg *et al* 2004, Cao *et al* 2021b). In this regard, measures of functional connectivity from scalp EEG recordings are of keen interest to elucidate the effect of neurodegeneration on intercommunications within widely distributed brain networks.

Analysing time-varying interactions and dynamic brain networks is increasingly attractive and challenging for researchers in the field of neurosciences (Li *et al* 2019). Recently, many techniques to estimate dynamic functional connectivity have been developed to extract biomarkers from EEG signals, including short-time Fourier transform (STFT) (Ahmadlou *et al* 2012, Keijzer *et al* 2021), wavelet analysis (Sankari and Adeli 2011, Handojoseno *et al* 2013, Jeong *et al* 2016, Ieracitano *et al* 2017), error reduction ratio (Zhao *et al* 2020) and Hilbert–Huang transforms (HHTs) (Shan *et al* 2021). Although those techniques are satisfactory to an extent and can be extended to estimate time-frequency coherence between different EEG channels, there are some limitations because of their principles. STFT computes Fourier spectra on successive sliding windows and the STFT mainly suffers from the trade-off between temporal and spectral resolution (Fu *et al* 2014, Moca *et al* 2021). Generally, STFT is employed to analyse the linear and non-stationary signals (Mousavi *et al* 2020). To avoid the window problem of STFT, wavelet analysis employs a longer window for lower frequencies and a shorter one for higher frequencies. In this case, it is more suitable for extracting time-varying information in different frequency bands (Sakkalis 2011). However, wavelet-based methods suffer from the Heisenberg uncertainty principle, the wavelet transform cannot achieve fine resolutions in both the time domain and frequency domain simultaneously due to non-adaptivity once the basis wavelet is set (Fu *et al* 2014). Wavelet transform is an advanced technique developed from Fourier analysis, using harmonic waves as its templates. Therefore, facing some similar problems of Fourier spectrum analysis, the wavelet is capable to solve inter-wave frequency modulation and cannot solve intra-wave frequency modulation (Shan *et al* 2021). However, neural oscillations have not been proved to be sinusoidal (Mazaheri and Jensen 2008, Jones 2016, Cohen 2017a). Wavelet-based approaches have the weakness of dealing with non-sinusoidal oscillations and discriminating them from sinusoidal ones (Cohen 2017b). Therefore, there is a need to develop novel methods to fully explore the

hidden association in the typical nonlinear and non-stationary EEG recordings. Unlike wavelet transform with sinusoidal templates, empirical mode decomposition (EMD) does not need any template assumption of the target signal (Huang *et al* 1998), which may improve the ability of extracting non-stationary and non-linear EEG information to an extent. EMD analyses the behaviour of non-stationary and non-linear signals by decomposing them into several intrinsic mode functions (IMFs) that could be further analysed by HHTs. Since the decomposition is based on the characteristics of the local time scale, with the HHT, the IMFs generate instantaneous frequencies (IFs) as functions of time that separately estimate dynamic structures of different transient information. Furthermore, Shan *et al* (2021) developed a new brain connectivity method relying on the revised HHT (RHHT) based on complete ensemble EMD (EEMD) with adaptive noise (CEEMDAN). It is able to capture dynamic interconnection between EEG signals and shows higher time-frequency resolution, compared with wavelet analysis. The 'mode mixing' is a non-negligible issue of the traditional EMD. To be more specific, one mode may represent different-amplitude oscillations or there are oscillations with high similarity found in different modes. To overcome this, Wu and Huang (2009) developed EEMD, which performs the EMD over an ensemble of the signal plus white Gaussian noise. However, there are still a variety of problems remaining and showing up. For instance, residual noise exists in IMF, and adding different white Gaussian noise to the signal increases the difficulty in controlling the number of IMFs. Torres *et al* (2011) improved the algorithm by proposing the CEEMDAN. The main improvement occurs in adding noise. CEEMDAN tries to add a distinct noise at each step of the decomposition process, while EEMD adds the white Gaussian noise after the extraction of each IMF.

Considering the aforementioned findings, it is hypothesised that the functional brain network connectivity of patients with AD differs from networks of age-matched healthy controls (HCs). The peak frequency extracted from the functional connectivity estimates is also hypothesised to act differentially for these two groups. The present study proposes a framework to accomplish the discrimination between AD and HCs based on wavelet cross-spectrum (WC) and RHHT cross-spectrum, the latter of which is used for the first time in the field of AD. The second innovation of this study is to evaluate a promising biomarker based on the peak frequency of cross-spectrums (PFoCSs). The proposed method is advanced in capturing dynamic interconnection between EEG signals and pointing out frequency-related biomarkers more precisely, which may help us to better understand brain dysfunction in AD. Then, a novel topographic visualisation method is designed to map the estimated brain connectivity. Finally, the proposed RHHT technique is critically compared with other approaches in terms of principles, results and limitations.

2. Materials and methodology

2.1. Experimental data and EEG pre-processing

Participants were recruited from Sheffield Teaching Hospitals NHS Foundation Trust Neurology clinics. HCs were enrolled through educational meetings, word of mouth, family and friends. The Sheffield Teaching Hospital memory clinic provided the majority of these patients. This is a young-onset memory clinic seeing people predominantly aged under 65. The study includes participants recruited between September 2014 to December 2019. Forty participants were recruited in this work (70 years > age > 48 years) and resting-state EEG recordings were undertaken from both cohorts by our research team based at the University of Sheffield. The subjects from both groups were age-matched, HC (12 female/8 male, mean age 61y, ±SD 6.7y), AD (8f/12m, 60y ± SD 4.4y). The EEG study underwent ethics approval by the Yorkshire and The Humber (Leeds West) Research Ethics Committee (reference number 14/YH/1070). AD patients had their diagnosis confirmed between 1 month and up to 2 years prior to their EEG recording while they had mild to moderate cognitive deficits, according to their Mini-mental state examination. All patients and controls had brain magnetic resonance imaging (MRI) scans to eliminate other alternative causes of dementia. For the age and gender-matched HC cohort, normal MRI brain scans and cognitive assessments were required before their EEG recordings. The final diagnosis of AD was based on the National Institute of Neurological and Communicative Disorders and Stroke and the Alzheimer's Disease and Related Disorders Association criteria (Dubois *et al* 2007); diagnosis was reached based on a consensus of multidisciplinary evidence, considering clinical history, neurological examination, neuropsychological scores and neuroradiological findings (Blackburn *et al* 2018).

The dataset includes 19 AD patients and 20 HC participants. EEG recordings were undertaken with an XLTEK 128-channel headbox (Optima Medical LTD) and Ag/AgCL electrodes at a sampling frequency of 2 kHz by implementing a modified 10–10 overlapping a 10–20 international system of electrode placement, with a referential montage (linked earlobe reference). Thirty-minute resting-state EEG recordings (task-free—participants were instructed to rest and refrain from thinking anything specific) were obtained from each participant including sustained periods of keeping their eyes closed (EC) alternating with periods during which they kept their eyes open (EO). The recordings obtained were subsequently reviewed by a neurophysiologist—on an XLTEK review station—and for each participant,

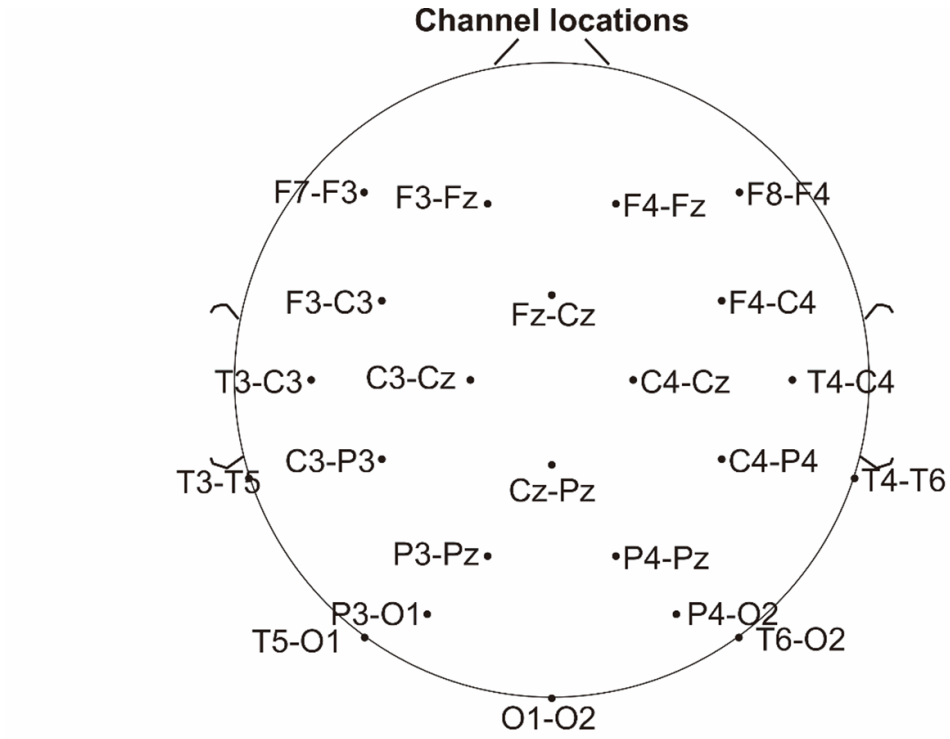

(A)

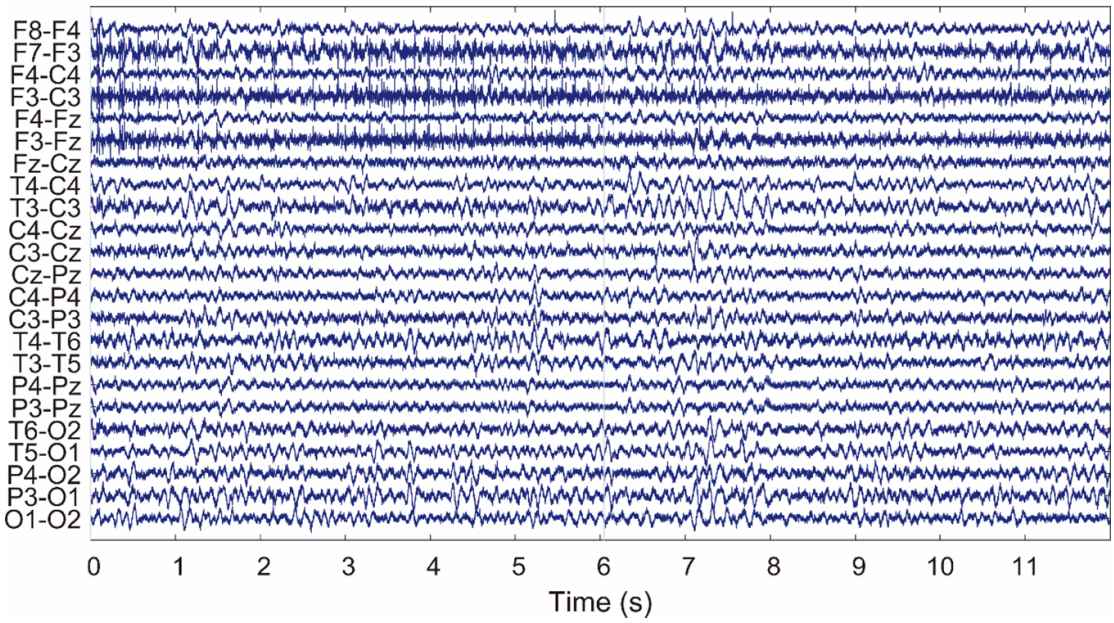

Figure 1. (A) Bipolar channel locations. The numbers 1, 2, 3, 4, 5, 6 and 7 represent the left frontal, right frontal, left temporal, right temporal, parietal, left occipital and right occipital regions, respectively (B) an example of 23-bipolar-channel EEG recordings.

three 12 s artefact-free mini-epochs of EC and EO were selected. To reduce volume conduction effects related to the common reference electrode, 23 bipolar derivations were created from different brain regions: the left frontal (F7–F3, F3–FZ), right frontal (F8–F4, F4–FZ), left frontocentral, temporo-central, temporal and centroparietal (F3–C3, T3–C3, T3–T5, C3–P3), right frontocentral, temporo-central, temporal and centroparietal (F4–C4, T4–C4, T4–T6, C4–P4), midline frontocentral, centroparietal and left and right parasagittal central regions (Fz–Cz, Cz–Pz, C3–Cz, C4–Cz), left parietal, parieto-occipital and temporo-occipital areas (P3–Pz, P3–O1, T5–O1), right parietal, parieto-occipital and temporo-occipital areas (P4–Pz, P4–O2, T6–O2) and midline occipital region (O1–O2)).

An example of the 23 bipolar channels used in this work and their locations are shown in figure 1. The functional connectivity is calculated by using each pair of EEG signals, and figure 2 shows the 253

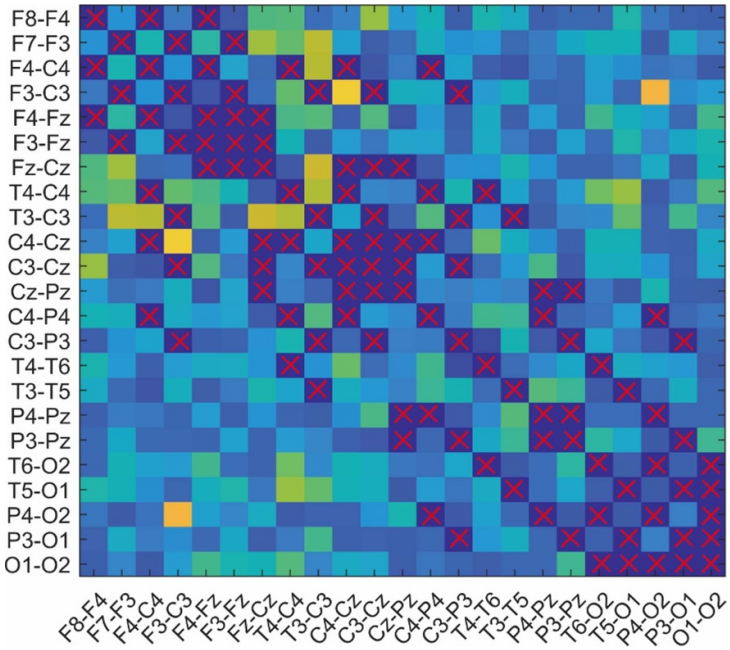

Figure 2. A total of 207 possible channel pair combinations and 46 discarded pairs marked with X (symmetry).

possible channel pair combinations $\left(C_2^{23}\right)$. It cannot be ignored that some combinations have common EEG channels because a bipolar approach is employed (such as F4–C4 and C4–P4), which may result in a misleading high false connectivity between some of the bipolar channels. To avoid this issue, the authors neglected any pair with common EEG electrodes. Therefore, the 46 channel pairs that have this characteristic include (F8–F4, F4–FZ), (F8–F4, F4–C4), (F7–F3, F3–FZ), (C4–CZ, CZ–PZ), (T4–C4, C4–P4), (F3–C3, T3–C3), (C4–P4, P4–PZ), (FZ–CZ, C4–CZ), (T3–T5, T5–O1), (C3–CZ, CZ–PZ), (P4–O2, O1–O2), (T6–O2, P4–O2), (T6–O2, O1–O2), (F7–F3, F3–C3), (F4–FZ, FZ–CZ), (T3–C3, C3–CZ), (F3–FZ, FZ–CZ), (T4–C4, T4–T6), (FZ–CZ, CZ–PZ), (C4–CZ, C3–CZ), (P3–PZ, P3–O1), (F3–C3, C3–P3), (F4–C4, F4–FZ), (F4–C4, T4–C4), (F4–C4, C4–CZ), (C3–P3, P3–O1), (C4–P4, P4–O2), (F4–C4, C4–P4), (T5–O1, O1–O2), (CZ–PZ, P4–PZ), (F3–C3, F3–FZ), (P4–PZ, P3–PZ), (F3–C3, C3–CZ), (F4–FZ, F3–FZ), (FZ–CZ, C3–CZ), (T4–C4, C4–CZ), (T3–C3, C3–P3), (T3–C3, T3–T5), (C4–CZ, C4–P4), (C3–CZ, C3–P3), (CZ–PZ, P3–PZ), (C3–P3, P3–PZ), (T4–T6, T6–O2), (P4–PZ, P4–O2), (T5–O1, P3–O1), (P3–O1, O1–O2) (Cao *et al* 2021a). In the following processes, only those pairs without common channels are considered, while the values of the 46 neglected channels are set as null (figure 2). Hence, 207 channel pairs are remaining for the following processing and discussion.

Figure 3 presents a flowchart of the proposed framework, including pre-processing, time-frequency brain connectivity analysis, feature extraction, significance test and machine learning classification. Before estimating brain connectivity, data were pre-processed by the following steps: (a) each signal was filtered to 0–50 Hz; (b) the recordings were down-sampled to 100 Hz to decrease computation cost.

2.2. Time-frequency brain connectivity methods

2.2.1. Wavelet-based cross-spectrum

The continuous wavelet transform (CWT) of a time series x is defined as:

$$\mathrm{CWT}_x(a,b) = \int_{-\infty}^{+\infty} x(t)\,\Psi^*_{a,b}(t)\,\mathrm{d}t \tag{1}$$

where Ψ is the mother wavelet, a is the scaling parameter and b is the shifting parameter. In this study, the Morlet wavelet was chosen as the mother wavelet because it is reasonably localised in both time and frequency (Ieracitano *et al* 2017). Each scale corresponds to a specific frequency value, so CWT is a function of time and frequency. The wavelet formulation of cross-spectrum between two signals, x and y, can be formulated as:

$$\mathrm{WC}_{xy}(a,b) = S\left(W_x(a,b)\,W_y^*(a,b)\right) \tag{2}$$

where $W_x(a,b)$, $W_y(a,b)$ are the wavelet transforms of x and y at scales a and position b; S denotes a function of smoothing, and * means complex conjugate.

Smoothing takes place across scale and time axes; it increases the degree of freedom for each point in the CWT (Sankari *et al* 2012). A proper smoothing function for WC application across time axis S_{time} is defined for the Morlet:

$$S_{\mathrm{time}}(\mathrm{CWT}(t,f)) = \mathrm{CWT}(t,f) \wedge c_1^{\frac{-\lambda^2}{2}} \tag{3}$$

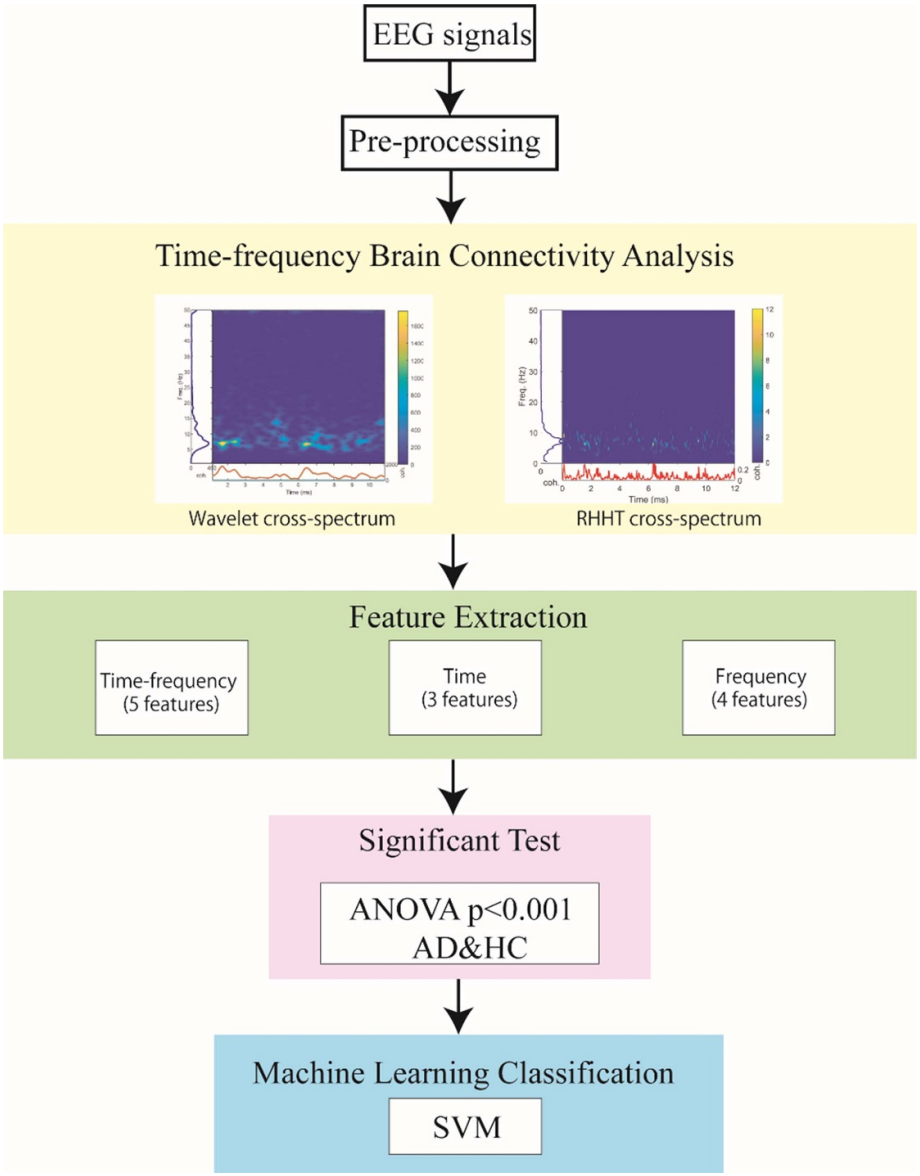

Figure 3. Flow diagram of the proposed framework.

where $\lambda = t/a$, c_1 is a normalisation constant, and $\wedge$ refers to the convolution operator. The smoothing function across scale S_{scale} (frequency) axis is defined as

$$S_{\text{scale}}\left(\text{CWT}\left(t,f\right)\right) = \text{CWT}\left(t,f\right) \wedge c_2 \prod\left(0.6a\right) \quad (4)$$

where c_2 is a normalisation constant, and $\prod$ is the rectangular function. In practice, the two convolutions in equations are computed discretely and the normalisation coefficients are determined numerically. The width of the rectangular function $\prod$ used in S_{scale} is determined by the scale-decorrelation length that is empirically determined to be 0.6 for the Morlet wavelet (Sankari *et al* 2012).

2.2.2. Revised Hilbert–Huang transformation (RHHT)-based cross-spectrum

Firstly, an advanced method of EMD is used to decompose each EEG signal, called CEEMDAN. In this case, we can obtain a series of complete and oscillatory components, named IMFs. Secondly, the HHT is performed on the IMFs of the signal to capture IF and amplitude features. Finally, the cross-spectrum of each pair of channels is calculated based on the HHT spectrum.

2.2.2.1. CEEMDAN

Given a signal $x(t)$, the defined operator $E_j(\cdot)$ produces the jth mode of $x(t)$ by EMD. Let $n^i \in [0, 1]$, $i = 1, \ldots, I$ be white noise where I is the realisation times of adding noise. Coefficient ε_i allows selecting the signal-to-noise ratio at each stage. The

implementation of the CEEMDAN algorithm can be summarised as follows:

(1) Decompose I realisations $x(t)+\varepsilon_0 n^i(t)$ by EMD to obtain the first mode $\widetilde{\mathrm{IMF}}_1$ that is defined as:

$$\widetilde{\mathrm{IMF}}_1 = \frac{1}{I}\sum_{i=1}^{I}\mathrm{IMF}_1{}^i. \tag{5}$$

(2) At the first stage ($j=1$) calculate the first residue $r_1(t)$:

$$r_1(t) = x(\mathrm{t}) - \widetilde{\mathrm{IMF}}_1. \tag{6}$$

(3) Decompose I realisations $r_1(t)+\varepsilon_1 E_1\left(n^i\right)$ by EMD to obtain their first modes and the second CEEMDAN mode $\widetilde{\mathrm{IMF}}_2$ is defined as:

$$\widetilde{\mathrm{IMF}}_2 = \frac{1}{I}\sum_{i=1}^{I} E_1\left(r_1(\mathrm{t}) + \varepsilon_1 E_1\left(n^i(\mathrm{t})\right)\right). \tag{7}$$

(4) For $j=2, 3\ldots I$, calculate the jth residue:

$$r_j(t) = r_{j-1}(\mathrm{t}) - \widetilde{\mathrm{IMF}}_j. \tag{8}$$

(5) Decompose realisations $r_j(t)+\varepsilon_j E_j\left(n^i(t)\right)$ by EMD to obtain their first modes and the $(j+1)$th CEEMDAN mode $\widetilde{\mathrm{IMF}}_{j+1}$ is defined as:

$$\widetilde{\mathrm{IMF}}_{j+1} = \frac{1}{I}\sum_{i=1}^{I} E_1\left(r_j(\mathrm{t}) + \varepsilon_j E_j\left(n^i(\mathrm{t})\right)\right). \tag{9}$$

(6) Go to step 4 for the next j and repeat steps 4 and 5 until the residue is no longer feasible to be decomposed (the residue does not have at least two extrema).

The final residual $R(t)$ is written as

$$R(t) = x(t) - \sum_{j=1}^{J}\widetilde{\mathrm{IMF}}_j \tag{10}$$

with j being the total number of modes. The given signal $x(t)$ can be expressed as:

$$x(t) = \sum_{j=1}^{J}\widetilde{\mathrm{IMF}}_j + R(t). \tag{11}$$

CEEMDAN needs to adjust its parameters to obtain a better decomposition of the data (Torres *et al* 2011, Mousavi *et al* 2020). Noise standard deviation (Nstd), the number of realisations (NR), and the maximum number of shifting iterations (MaxIter) are important parameters for optimising the results of decomposition (Mousavi *et al* 2020). Figure 4 shows the flowchart of the CEEMDAN algorithm. Three parameters control the process of CEEMDAN. To be more specific, noise standard deviation (Nstd) represents the strength of the added white noise. The number of realisations (NR) controls the number of adding noise. The maximum number of shifting iterations (MaxIter) indicates the number of decompositions. In the present study, considering both computation efficiency and separation accuracy, these parameters were set as: Nstd = 0.1, NR = 100, and MaxIter = 1000.

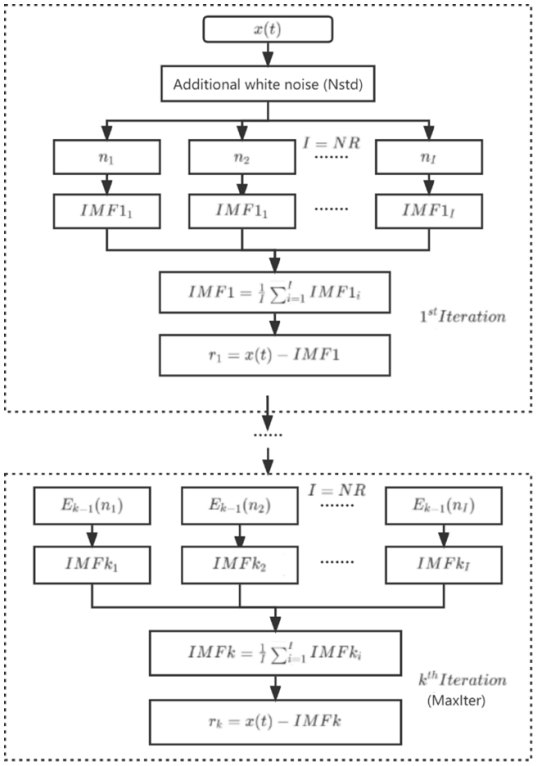

Figure 4. Flowchart of CEEMDAN algorithm.

2.2.2.2. Hilbert–Huang transform (HHT)

Then, the Hilbert transform (HT) is applied to each IMF to obtain IFs and instantaneous amplitude features. This eventually yields a time-frequency representation (Hilbert spectrum) for each IMF. For an original signal $x(t)$, its HT $h(t)$ is obtained by (Huang *et al* 1998):

$$h(t) = \mathrm{HT}(x(t)) = \frac{1}{\pi}\mathrm{P.V.}\int_{-\infty}^{\infty}\frac{x(\tau)}{t-\tau}\mathrm{d}\tau \tag{12}$$

where P.V. denotes the Cauchy principal value, t is the time variable and τ is the time interval. In this case, the HHT of the signal is given as follows:

$$z(t) = x(t) + ih(t) = a(t)\,\mathrm{e}^{\mathrm{i}\theta(t)} \tag{13}$$

where $a(t)$ and $\theta(t)$ denote the amplitude and phase, respectively.

$a(t)$ is the trace envelope and defined as:

$$a(t) = \sqrt{x^2(t) + h^2(t)}. \tag{14}$$

$\theta(t)$ is defined as:

$$\theta(t) = \arctan\left(\frac{h(t)}{x(t)}\right). \tag{15}$$

IF $f(t)$ is defined as the first derivative of $\theta(t)$. Thus,

$$f(t) = \frac{1}{2\pi}\frac{\mathrm{d}\theta(t)}{\mathrm{d}t}. \tag{16}$$

To prevent ambiguities because of phase unwrapping in equation (14), $f(t)$ can be calculated instead from:

$$f(t) = \frac{1}{2\pi}\frac{x(t)h'(t) - x'(t)h(t)}{x^2(t) + h^2(t)} \tag{17}$$

where the prime denotes derivative with respect to time. The time-frequency spectrum of signal $x(t)$ is defined as:

$$\mathrm{RHHT}_x(t, f(t)) = a(t)\,\mathrm{e}^{\mathrm{i}\theta(t)}. \tag{18}$$

The time-frequency spectrum of $\widetilde{\mathrm{IMF}}_j(t)$, t = 1, . . . , N, and $j = 1, \ldots, J$, and RHHT (t) are defined as:

$$\mathrm{RHHT}_{\widetilde{\mathrm{IMF}}_j}\left(t, f_j(t)\right) = a_j(t)\,e^{i\theta_j(t)} \tag{19}$$

$$\mathrm{RHHT}_R(t, f_R(t)) = a_R(t)\,\mathrm{e}^{\mathrm{i}\theta_R(t)}. \tag{20}$$

The time-frequency spectrum of $x(t)$ is:

$$\mathrm{RHHT}_x(t, f(t)) = \sum_{k=1}^{K} a_J(t)\,\mathrm{e}^{\mathrm{i}\theta_k(t)} + a_R(t)\,\mathrm{e}^{\mathrm{i}\theta_R(t)}. \tag{21}$$

A series of IFs are generated from the process, empowering the capability of in-depth signal analysis. At each time point, the number of IFs is corresponding to the number of IMFs. The RHHT method can generate a dozen of IMFs, which results in sparse time-frequency representations.

2.2.2.3. RHHT cross-spectrum

The RHHT cross-spectrum of $x(t)$ and $y(t)$ is defined as follows:

$$\mathrm{RC}_{xy}(t, f) = \int_{t-\delta/2}^{t-\delta/2} \mathrm{RHHT}_x(\tau, f) \cdot \mathrm{RHHT}_y{}^*(\tau, f)\,\mathrm{d}\tau \tag{22}$$

where, $\mathrm{RHHT}_{x_1}(\tau, f)$ and $\mathrm{RHHT}_y(\tau, f)$ are the RHHT coefficients of $x(t)$ and $y(t)$ and; $*$ means complex conjugate; δ is the length of the integrating range.

For RHHT cross-spectrum, the selection of δ is entirely empirical, independent of frequency. Different values of δ were used and the performance varied in terms of time-frequency resolution and computation cost. In this paper, the length of the integral window of RHHT coherence was set to 4. Given two signals $x(t)$ and $y(t)$, for all IMFs of $x(t)$ and $y(t)$, the RHHT cross-spectrums between $\widetilde{\mathrm{IMF}}_{xj}(t)$ and $\widetilde{\mathrm{IMF}}_{yj}(t)$ can be calculated and analysed separately. An example of RHHT and cross-spectrum is illustrated in figures S1 and S2 in supplementary.

2.2.3. Feature extraction

As shown in figure 3, both WC and RHHT methods yield a two-dimensional time-frequency cross-spectrum. To reveal the distribution of cross-spectrum in time (horizontal) and frequency (vertical) direction, the average was taken for two techniques, respectively (equations (21)–(24)):

$$\mathrm{WC}_{\mathrm{fre}}(f) = \frac{1}{t_{\max}}\sum_{t=0}^{t_{\max}} \mathrm{WC}(t, f) \tag{23}$$

$$\mathrm{WC}_{\mathrm{time}}(t) = \frac{1}{f_{\max}}\sum_{f=0}^{f_{\max}} \mathrm{WC}(t, f) \tag{24}$$

$$\mathrm{RC}_{\mathrm{fre}}(f) = \frac{1}{t_{\max}}\sum_{t=0}^{t_{\max}} \mathrm{RC}(t, f) \tag{25}$$

$$\mathrm{RC}_{\mathrm{time}}(t) = \frac{1}{f_{\max}}\sum_{f=0}^{f_{\max}} \mathrm{RC}(t, f). \tag{26}$$

In this case, 12 features were captured from the cross-spectrum map and two average curves (table 1).

2.3. Single-channel methods

To compare the efficiency and ability of the developed RHHT technique and PFoCS features to a non-connectivity method, PSD was calculated and then the same SVM classifier was applied. The PSD tends to be used to extract features from each band of the EEG recordings. Specifically, PSD in each trial was calculated for each of the 23 channels using Welch's method with 0.5 s windows, 50% overlap and 256 points. Then, power was averaged for Delta (0–4 Hz), Theta (4–8 Hz), Alpha (8–12 Hz) and Beta (12–32 Hz) and Gamma (32–45 Hz) frequency bands.

2.4. Statistical analysis

One-way analysis of variance (ANOVA) was employed to evaluate the significance of differences in the investigated features of AD vs HC. In this case, it guides to select channels for each frequency band based on the p-value, preparing for optimising the input features of machine learning. ANOVA is widely used to test the significant difference between the AD and HC groups (Sankari *et al* 2011, Engels *et al* 2015, Benwell *et al* 2020). ANOVA tests the null

Table 1. Extracted features from the cross-spectrum and two average curves.

Representations	Features				
WC and RC	Max	Peak frequency	Mean	Max/Mean	Std
WC_{fre} and RC_{fre}	Max	Peak frequency	Std	Max/Mean	
WC_{time} and RC_{time}	Max	Std	Max/Mean		

Max: the maximum value of the cross-spectrum or average curve, Std: the standard deviation of the cross-spectrum or average curve, Mean: the average of the cross-spectrum or average curve.

hypothesis, i.e. means of the tested groups are equal and the p-value indicates the statistical significance. Rejection of the null hypothesis leads to the conclusion that the two groups are statistically different (Cao *et al* 2021a). Before applying ANOVA, the parametric test assumptions have been tested. It has been found that the majority of features meet the assumptions but not all of them. To simplify the problem, we used the ANOVA analysis. To select promising features that offer significant differentiation between AD and HC and to reduce the computational burden of machine learning, the estimation was undertaken using a threshold $p < 0.001$. All statistical analysis was applied in MATLAB 2019b.

2.5. Machine learning

2.5.1. Features selection

Features were computed between all possible pairs of channels for each of the six independent EEG frequency bands for each subject: Delta (0–4 Hz), Theta (4–8 Hz), Alpha (8–12 Hz), Beta (12–32 Hz), Gamma (32–45 Hz) and Full (0–45 HZ). There were in total $207 \times 6 \times 12 = 14\ 904$ (channel × band × features) features extracted from WC and RHHT cross-spectrum respectively. If a feature is successfully passed through the significance test ($p < 0.001$, ANOVA), it would become an input to the machine learning classifier, as it indicates AD and HCs have a significant difference in terms of this feature. Each feature was normalised to $[-1, 1]$ for the AD and HC groups in preparation for machine learning classification.

2.5.2. Classifier

The SVM was applied to achieve the classification of AD and HC. SVM constructs an optimal separating hyper-plane in the feature space based on the structure risk minimisation principle (Fu *et al* 2014). The optimised features extracted from RHHT and WC in six bands are fed into the SVM with a radial basis function (RBF) kernel. Different machine learning algorithms were tested and compared, such as KNN, decision tree and SVM, etc. SVM outperforms other methods in terms of classification. Hence, this paper mainly utilises the SVM with RBF to represent classification results.

2.5.3. Cross-validation

The data from all subjects were mixed up and grouped by the eye state: EC, EO and EC&EO state. To avoid the problem of overfitting in the case of limited data as well as decrease the influence of selecting a training set, a five-fold cross-validation technique is employed. To be more specific, the dataset of each condition was divided into five subsets. Then five iterations are undertaken to ensure each subset is used for training and testing (Berrar 2019, Cao *et al* 2021a). That is to say, for each iteration, 80% of the dataset is used for training and the remaining 20% of the dataset is used for testing. Consequently, the classification result is calculated by averaging the accuracies obtained from five iterations.

3. Results

3.1. Machine learning classification

The ten pairs with the highest classification accuracy were chosen to evaluate the efficiency of WC and RHHT cross-spectrum methods in EO, EC and EO&EC states separately (figure 5). It can be observed that RHHT performs better in the Full band for all three eye states. It can achieve about 86% and 89% classification accuracy in EO and EC respectively, while features from the wavelet analysis can only provide classification accuracy of less than 85%. Besides, for the EC condition, the mean and median accuracies of RHHT lay closely to about 85%, which is relatively higher than the results obtained from the wavelet-based method (78%). Notably, the peak frequency of the frequency-average curve in the Full band most accurately discriminated the AD from the HC group in EO, EC and EO&EC conditions, and RHHT enables the Full band to consistently outperform other bands with respect to both highest and mean accuracy. However, for the WC method in EO and EO&EC states, the Theta band was superior to other bands, and the best feature was in the Theta band. In the meantime, WC only surpassed RHHT in the Theta and Beta band, while RHHT increased the accuracy in the Delta and Alpha band, especially for the EO Group with an approximate 5% increase.

It is noteworthy that the functional connectivity estimates, between the frontocentral midline and occipital derivations, demonstrate the highest accuracy in the Full band in all three eye conditions. For example, the RHHT PFoCS of the pair Fz–Cz:O1–O2 achieved the best classification performance with about 89% accuracy using the proposed machine learning method, which surpasses all features extracted from the wavelet-based method. Therefore, more

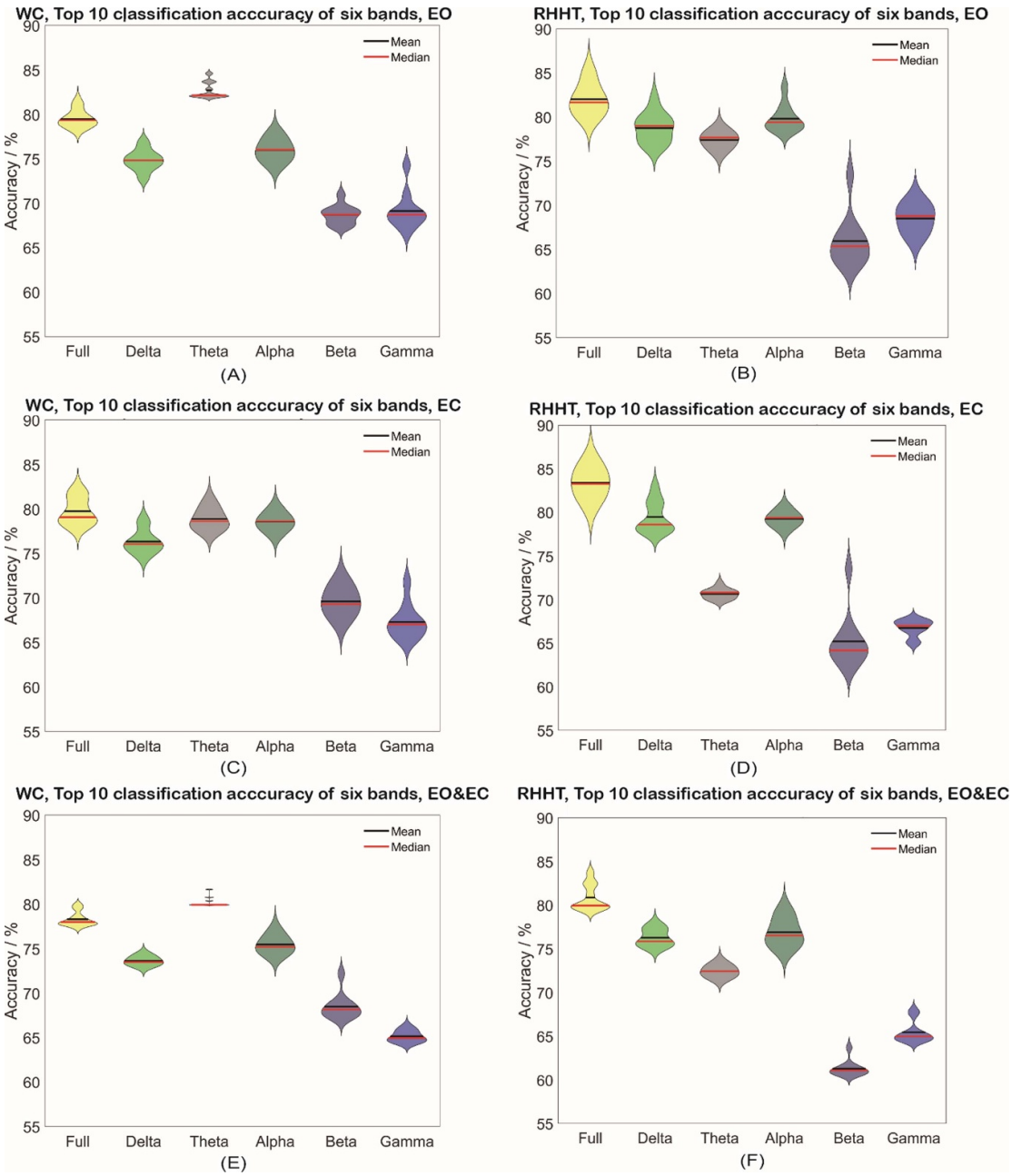

Figure 5. Top ten classification accuracies in EO (A), (B), EC (C), (D) and EO&EC (E), (F) using features from wavelet (left column) and RHHT cross-spectrum (right column).

details and analysis with respect to the Fz–Cz:O1–O2 connections are further discussed below.

3.2. Time-frequency functional connectivity

To evaluate the efficiency of the wavelet and RHHT-based methods, the time-frequency analysis is implemented on each channel pair. Figure 7 represents the cross-spectrum of Fz–Cz:O1–O2 obtained from wavelet (A) and (B) and RHHT (C) and (D), as well as the average value in time and frequency axes. It is obvious that the frequency resolution of RHHT is higher than the WC for both AD and HC participants. For instance, the WC method suggests that the PFoCS is located in the Alpha band (figure 6(A)), while RHHT is capable to indicate a specific frequency of 10 Hz (figure 6(C)). Similarly, figures 6(B) and (D) also exhibit the same pattern in the AD case. Furthermore, it can be observed that both two methods have dominating power in the Alpha band. Based on the resulting cross-spectrum of the channel pair Fz–Cz:O1–O2, the PFoCS of the AD subject is lower than the value of the HC subject, observed both from the wavelet and the RHHT cross-spectrum.

Figure 6(E) plots the distribution of the PFoCS value of each sample for the Fz–Cz:O1–O2 channel pair. For both RHHT and WC, there was a significant difference in the PFoCS ($p < 0.0001$, ANOVA). For both methods, the PFoCS for HCs ranges between 8 and 14 Hz with an average of 10 Hz, while the AD PFoCS varies from 4 to 12 Hz with an average of

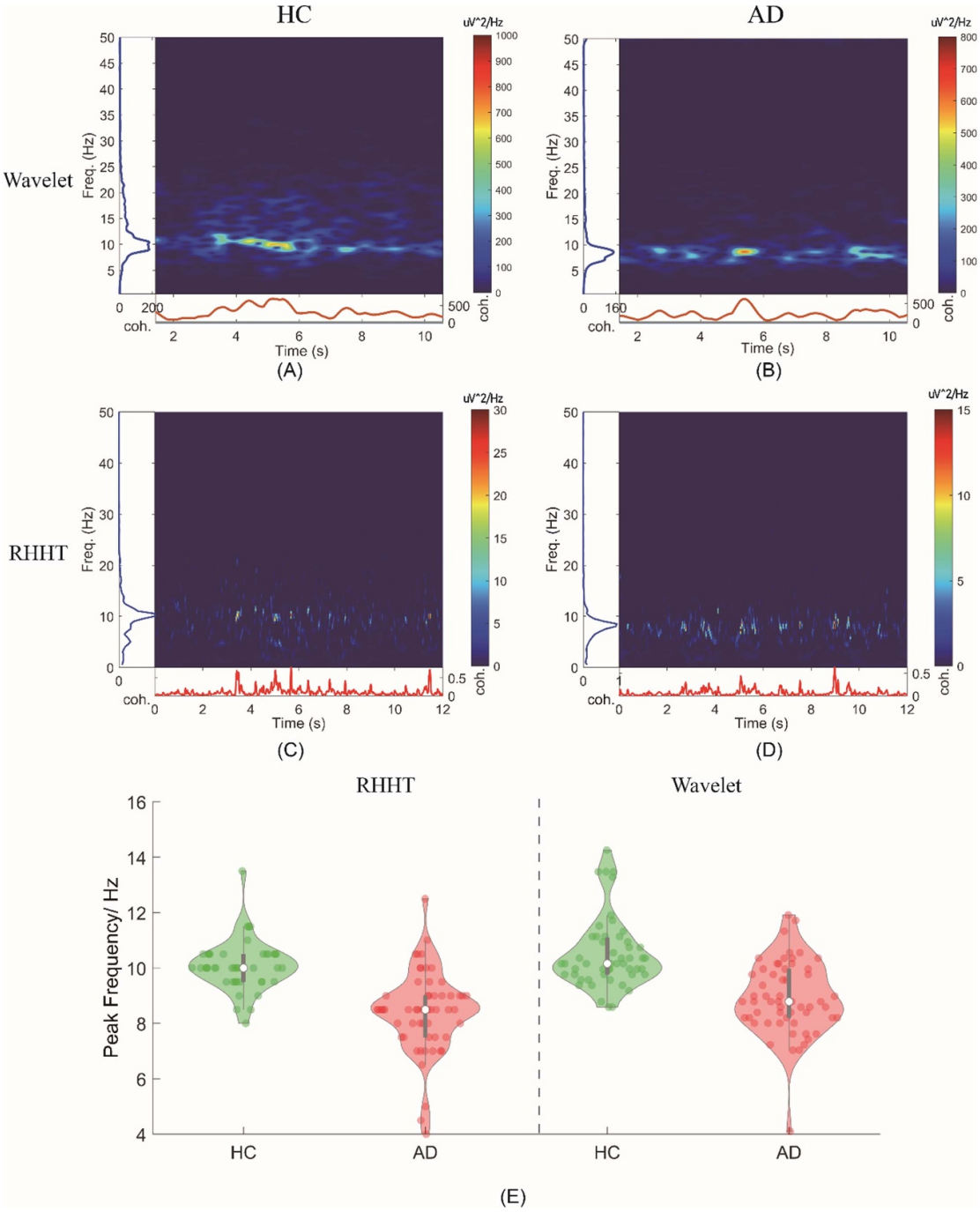

Figure 6. Time-frequency brain connectivity analysis of channel pair Fz–Cz:O1–O2. (A) WC for a HC participant. (B) WC for an AD participant. (C) RHHT cross-spectrum for a HC participant. (D) RHHT cross-spectrum for an AD participant. (E) A violin plot to present peak frequency values for channel pair Fz–Cz:O1–O2 ($p < 0.0001$, ANOVA).

8.5 Hz. Notably, compared with HCs, a majority of AD participants have an obvious decrease in terms of PFoCS in the Alpha band, and RHHT seems to outperform WT in detecting the difference to an extent since the p-value of RHHT (2.7×10^{-7}) is lower than the p-value of WT (5.6×10^{-5}). Consequently, the classification accuracy can be improved by using the RHHT technique. Moreover, the value of PFoCS varies in different bands, although it was mainly concentrated in the Alpha band. This may explain that the feature extracted from the Full band outperformed the Alpha band to some extent.

3.3. Topographic visualisation of PFoCS

To further compare the difference between AD and HCs across different brain areas, a novel visualisation method based on a topographic map is proposed to illustrate an extensive brain connectivity map. Figure 7 represents the occipital-related connectivity using the PFoCS as an estimation. The topography map represents the distribution of Full-band functional connectivity between channel O1–O2 and every other derivation included in this work. The channel O1–O2 and other contiguous channels that share a common electrode are set to NaN in the

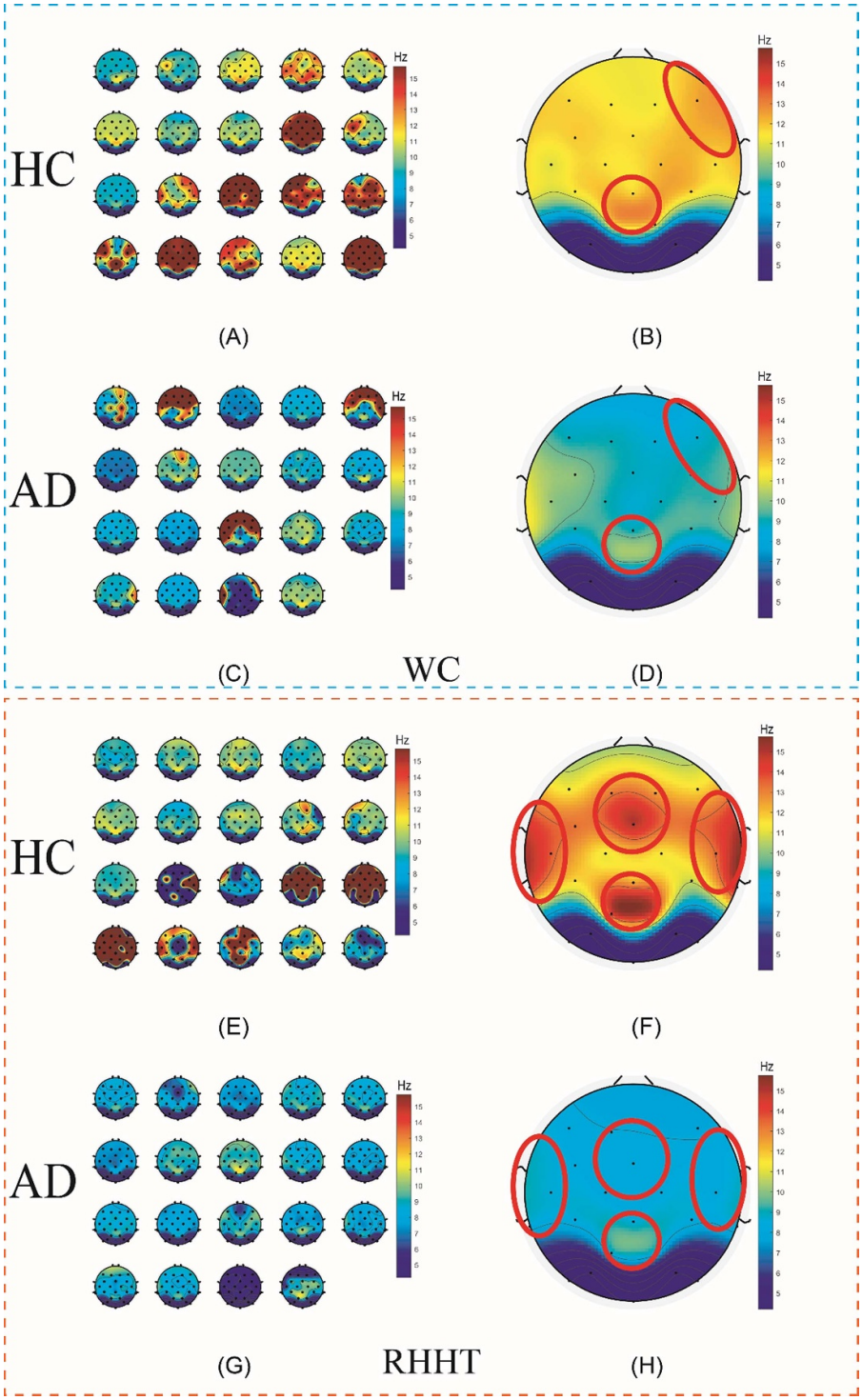

Figure 7. Topographic plots representing full-band connectivity PFoCS for each participant (left) and average (right) extracted by wavelet and RHHT techniques, by using each available derivation against the occipital O1–O2 channel (red circles indicates the areas that represent obvious difference between HC and AD).

resulting map (i.e. P3–O1, T6–O2, T5–O1, and P4–O2). On one hand, from the averaged topographic map, it can be observed that not only Fz–Cz:O1–O2 can significantly differentiate AD from HCs, but also many other areas show increased levels of PFoCS functional connectivity, offering a visual representation of the striking differences between AD and HC, clearly more prominent for the averaged RHHT-based maps. The red circles in figure 7 indicate the areas that represent the obvious difference between HC and AD. For instance, WC suggests the PFoCS of HC is about 4 Hz higher than AD in the right frontal and centroparietal region (figures 7(B) and (D)), while RHHT indicates the PFoCS of HC is about 6.5 Hz higher than AD in the right frontal, midline frontocentral, left frontocentral and centroparietal region (figures 7(F) and (H)). Clearly, the RHHT method suggests more differences between the two

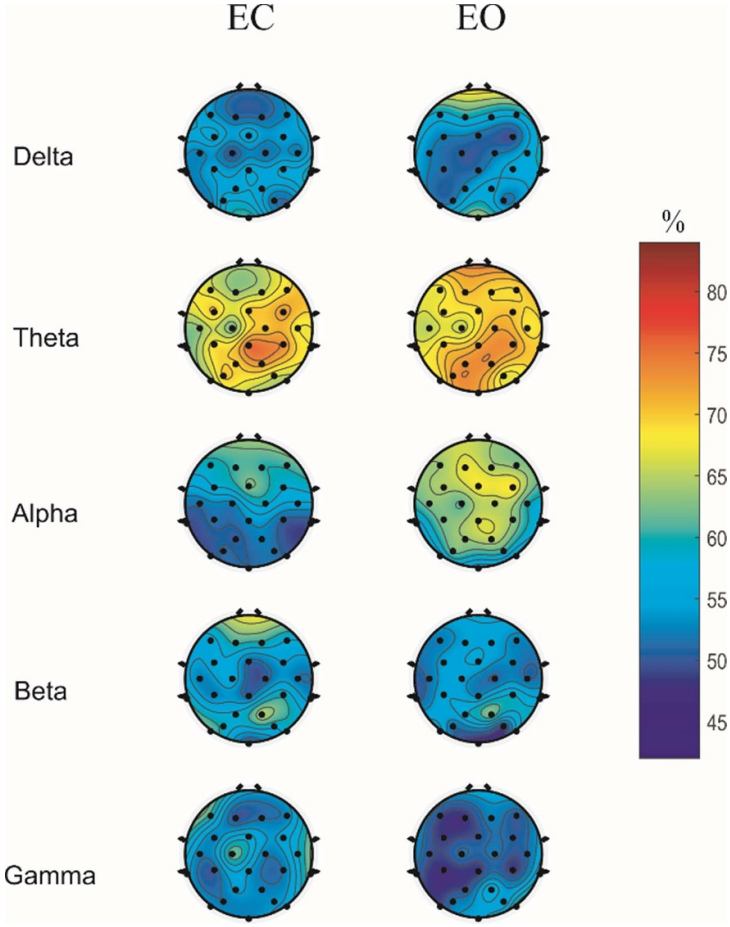

Figure 8. Topographic map of the classification accuracy using PSD.

groups in terms of values and regions. Those findings are in keeping with the previous significance test results and SVM-based classification.

On the other hand, the variations of estimated distribution for the participants are quite large. This is a general issue in EEG research since EEG has been associated with cognitive, emotional, and motor processes (Bell and Cuevas 2012). In this respect, participants from the AD and HC groups may have similar characteristics. As a result, the machine learning classifier cannot achieve 100% discrimination between the two cohorts. However, a similar trend can be observed as AD patients have relatively lower PFoCS across widely distributed brain areas. To be more specific, RHHT performed better in revealing the difference between AD and HCs in terms of the PFoCS, resulting from its superior time-frequency resolution and ability to estimate a frequency value.

3.4. PSD results

The spatial distribution of the classification accuracy is displayed in figure 8. Obviously, the most significant difference occurs in the Theta band. Noticeably, the highest accuracy is approximately 72%. The results obtained by PSD are about 15% lower than that of the RHHT method. That is to say, AD, the most common neurodegenerative disorder, affects not only the function of individual cortical regions but also the intercommunications between them. Furthermore, the abnormalities of AD brain connectivity are more prominent in the present dataset, which is satisfactorily evaluated by the proposed RHHT method.

4. Discussion

4.1. RHHT vs WC

EEG signals are often non-stationary in nature, contain non-linear processes, and their frequency components dynamically change over time (Lakshmi *et al* 2014, Yao and Wang 2017, Lotte *et al* 2018). Hence, the desired time-frequency analysis methods for qEEG studies should have satisfying resolutions in both the time and frequency domains. RHHT can clearly present the cross-spectrum distribution with time and frequency and localise any event on its occurring time as well as its IF (Peng *et al* 2005, Law *et al* 2012). Specifically, the PFoCS variation of RHHT shows a much higher resolution in comparison to those achieved by the Morlet wavelet spectrum. In this case, even though WC can achieve about 85% classification accuracy in the EO condition using the mean of cross-spectrum as a feature, it cannot

perform better when it comes to PFoCS. Figure S3 in the supplementary represents a brain connectivity map using the mean cross-spectrum of WC as an estimation. Consequently, RHHT is more suited for EEG brain connectivity analysis in this paradigm and performs better in localising in time PFoCS connectivity strength which is translated into better performance in distinguishing between AD and HCs.

Furthermore, the two techniques did not obtain satisfying outcomes when high-frequency bands (Beta and Gamma) were analysed in isolation, which suggests the effect of AD on the high-frequency bands cannot be tracked with the WC and RHHT techniques. Those results agree with several previous works that focus on the peak frequency. For instance, Scally *et al* (2018) provided evidence that peak frequency brain connectivity in the range of 6–14 Hz is associated with ageing. Barry and de Blasio (2017) revealed a significant difference between young and older adults in the Delta, Theta and Alpha bands. Therefore, it seems that with some methods cognitive performance and neurodegeneration are more related to the change in the low-frequency band rather than the Beta and Gamma band (Posthuma *et al* 2001, Smit *et al* 2006, Nir *et al* 2010, Grandy *et al* 2013).

4.2. RHHT vs other functional connectivity methods

In addition to the aforementioned advantages, the RHHT method can track non-linear associations between channels. To demonstrate the superior performance of cross-spectrum RHHT, in distinguishing between AD and HCs, we compared our findings against those obtained by implementing other popular linear and non-linear brain connectivity methods. Phase locking value (PLV) (Lachaux *et al* 1999, Hassan *et al* 2017) and mutual information (MI) (Wells 1996, Melia *et al* 2015, Nimmy *et al* 2019) were used to estimate non-linear connections, while Pearson correlation coefficient (van Mierlo *et al* 2014, Chen *et al* 2018) and magnitude squared coherence (MSC) (Pfurtscheller and Andrew 1999, Cao *et al* 2021a) were calculated with respect to linear brain connectivity. MI measure indicates the mutual dependence of two signals, i.e. how much information is shared between two signals (Cover and Thomas 2005). It is based on a probability function and entropy. Three features are taken from the cross-correlation, namely the maximum value of correlation (CorrMax), the mean value of correlation (CorrMean) and the correlation lag at the maximum value of correlation (CorrLag). Two features are taken from the MSC: maximum (CohMax) and mean values (CohMean). PLV measures the significance of the phase covariance between two signals. PLV values are in the range from 0 to 1. If the phase difference of the two signals remains the same, PLV is close to one. A PLV close to zero indicates that there is no phase synchrony between two signals (Cao *et al* 2021a). Figure 9 illustrates the comparison between the proposed methods and conventional techniques in terms of the top ten channel classification accuracies. The average, highest and lowest accuracy are represented by the bar chart. To statistically compare different techniques, the Mann–Whitney U tends to be more appropriate as the top ten accuracies do not meet the parametric assumptions of a normal distribution (Shan *et al* 2021). The Mann–Whitney U test tests the null hypothesis that data in two groups are samples from continuous distributions with equal medians, against the alternative that they are not. The test assumes that the two samples are independent. The Mann–Whitney test was applied to check for significant differences between the accuracies of techniques, using a threshold of $p < 0.001$. Overall, the EO condition appears more suitable to distinguish AD patients from HCs, since the classification accuracy is slightly higher in comparison to the EC recordings. For the EC condition (figure 9(A)), as expected, RHHT and WC were superior in comparison to others, especially in the Full band, as well as Delta and Alpha bands. RHHT performs significantly better than others in the Full band (the accuracy ranges between 84% and 88%), while WC provides significantly higher accuracy in the Theta band (78%–82%). For the EC condition (figure 9(B)), RHHT significantly outperforms other methods in the Full (83%–89%), Delta (76%–82%) and Alpha bands (77%–82%). WC keeps its significant superiority in the Theta band, which ranges from 84% to 87%. Therefore, our findings suggests that the non-linear time-frequency method (RHHT) has superior performance in the Full, Delta and Alpha band that contributes in better differentiating AD participants from HCs, as there is a 10%–20% improvement in classification accuracy. Although the lower frequency bands have a higher contribution to the classification than the higher frequency bands, there is still evidence that higher frequency bands can be useful (Poil *et al* 2013, Babiloni *et al* 2016). The full band higher classification accuracy with RHHT might also be related to the ability of the technique to increase the signal-noise-ratio of high-frequencies and extract additional useful frequency features. To explore the evidence, we used 0–12 Hz as a separate band and performed the same method on it. The results are shown in figure S4 of supplementary. It can be found that '0–12 Hz' outperforms every single band, but its accuracies are slightly lower than the Full band (0–45 Hz). In this case, RHHT in the Full band can provide more information on the discrimination between AD and HC than 0–12 Hz. RHHT probably can increase the signal-noise-ratio of high-frequency data which extracts useful frequency features for higher classification accuracy and compresses the noise. The advantages of the proposed RHHT method rely on its distinct signal decomposition and higher resolution in the time and frequency domain.

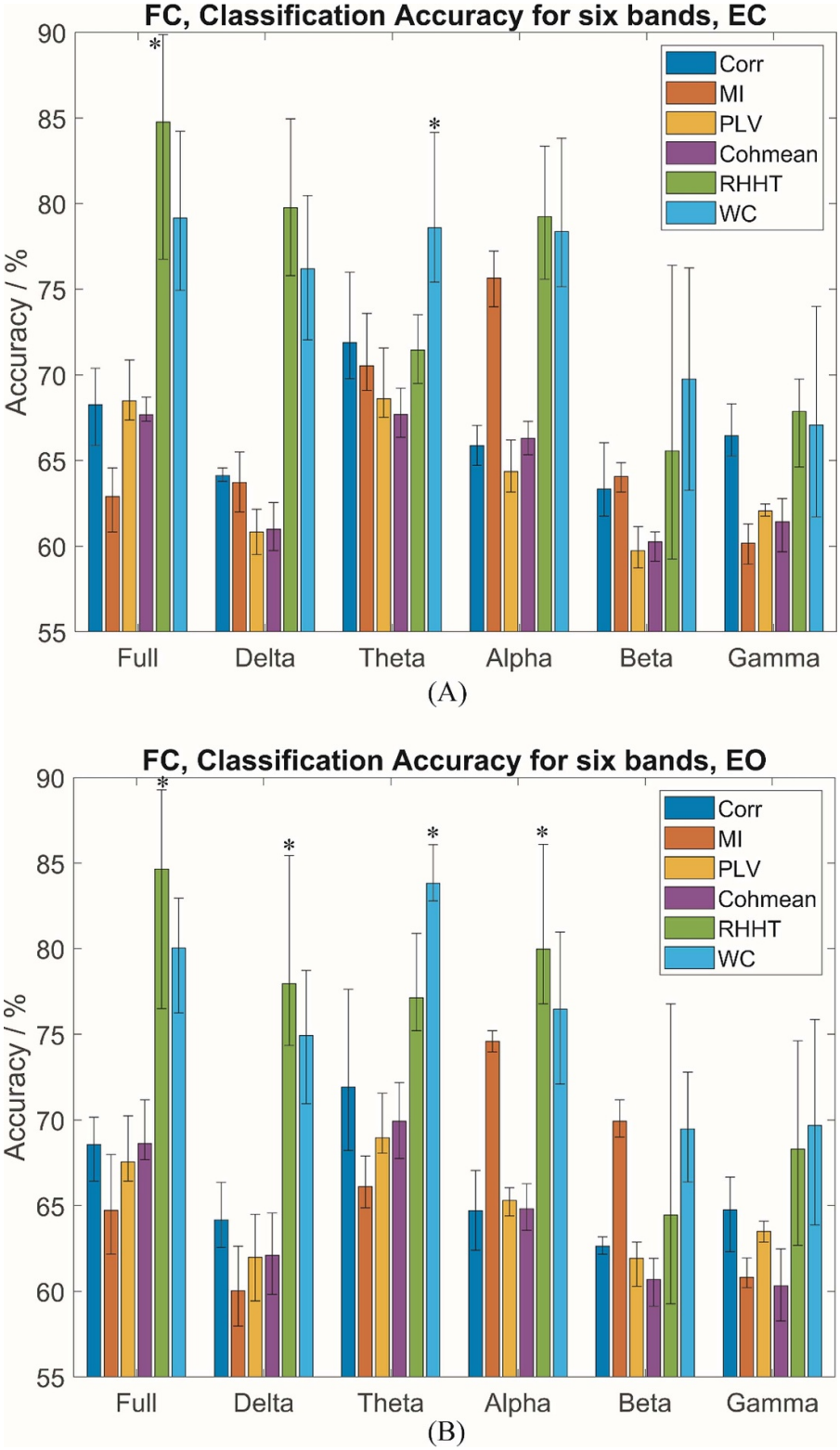

Figure 9. Comparison of the RHHT and previous brain connectivity methods. * Mann–Whitney test, $p < 0.001$, it means significant outperformance in a band.

Our study is undertaken on resting-state EEG recordings and Engel *et al* (2013) in their pivotal work introduce the concept of 'intrinsic coupling modes' to denote complex spectral and spatial signatures, likely dynamic in nature that characterise brain coupling not enforced by a stimulus or task. They also highlight how phase and amplitude-based functional connectivity measures have the potential to capture various pathophysiological and neurophysiological aspects of brain function (Engel *et al* 2013). RHHT cross-spectrum has the ability to capture both phase and amplitude coupling. Under this

prism, the dynamic properties of RHHT offer the resolution required to capture various intrinsic coupling modes and translate into higher classification performance like the one observed with the PFoCS.

4.3. RHHT vs single-channel method

This paper demonstrates that RHHT cross-spectrum, a functional brain connectivity method implemented in this work to produce strength of associations between multiple EEG channels, could produce a higher classification accuracy in distinguishing AD participants from a group of age-matched HCs, compared to single-channel methods like PSD. PSD is a widely-used single-channel method dealing with EEG recordings, which calculates the distribution of power against the frequencies. Furthermore, the spectral information in different bands can be estimated by PSD. It normally considers Delta, Theta, Alpha, Beta and Gamma bands for EEG, since those bands represent distinct neural activities (Wang *et al* 2015a, 2015b, 2017, Liu *et al* 2016). Many previous works have shown that PSD can be used to evaluate the changes between HC and AD groups. For example, it was found that AD groups have relatively higher PSD than HC groups in the Theta band (4–8 Hz), while AD patients may experience a decrease in Alpha power (8–12 Hz) and Beta power (12–32 Hz) (Liu *et al* 2016, Benwell *et al* 2020).

Table 2 compares the highest classification results of the popular features extracted from EEG in the literature and the approach proposes in this paper, using the same dataset of AD and HCs. Evidently, the developed method obtains the highest accuracy, which is clearly higher than other existing approaches. Notably, the time-frequency methods (i.e. WC and RHHT) perform better than other methods that focus on stationary information with the superiority at approximately 10%. That is to say, dynamic and non-stationary methods may have more potential to reveal hidden changes during the progress of neurodegeneration.

Table 2. A comparison of performances of the various functional connectivity methods and univariate methods (maximum accuracy achieved by each method).

Features	References	SVM accuracy
PSD	Wang *et al* (2017), Benwell *et al* (2020)	72.2%
Correlation	Chen *et al* (2018)	77.7%
Coherence	Sankari *et al* (2011), Wang *et al* (2015b)	72.11%
Mutual information (MI)	Babiloni *et al* (2016), Nimmy *et al* (2019)	77.23%
Phase locking value (PLV)	Engels *et al* (2015), Kabbara *et al* (2017), Su *et al* (2021)	72.11%
WC	Sankari and Adeli (2011)	85.2%
RHHT—PFoCS	This paper	88.9%

4.4. Limitations and future direction

However, the proposed framework has several challenges to address in future research. Firstly, the computation efficiency of the RHHT technique is not satisfying. It could be improved to meet the requirement of real-time feedback, aiming to translate it into a clinically useful diagnostic tool. Secondly, the training dataset for machine learning is not cross-subject, limiting the universality of the proposed algorithm. Cross-subject validation means that the data for training and testing are extracted from different participants. Only this type of approach can demonstrate the universality of the proposed methods, but it usually requires a significant number of participants to reveal the degree of variability between subjects. In the present study, the size of the dataset is limited. The cross-subject approach is not appropriate to evaluate the model performance and therefore has not been applied. In this case, the data from all subjects were mixed up and then divided into training and testing. Thirdly, to reduce volume conduction effects from a common reference, bipolar derivations were used to assess the degree of differences between various pairs of electrodes for two different cohorts of subjects. With this approach—the use of bipolar pairs of electrodes—the effects of volume conduction are reduced but not eliminated. We recognise that this work is based on a sensor-level scalp EEG analysis, and we do not claim to be able to precisely localise the spatial characteristics underpinning the EEG sensor findings. Fourthly, the noise tolerating capability of the RHHT technique may need to be further studied. According to our previous study, the performance of RHHT seems to be more sensitive to noise (Shan *et al* 2021). Finally, only a two-group classification (HCs vs AD) has been carried out in the present study, without considering preclinical or prodromal populations or staging of disease severity of AD patients. The proposed method has demonstrated effective performance in the case of HCs vs AD and it may have potential in dealing with the classification of HCs vs MCI vs AD. We are collecting data from MCI and this three-class classification will be tested in further studies.

5. Conclusion

In this study, we demonstrate that the peak frequency estimated with the RHHT-based brain functional connectivity is reduced in a group of AD patients in comparison to an age-matched HC cohort. A comparison undertaken with various other linear and nonlinear functional connectivity EEG methods shows that RHHT is better suited to detect this difference, because of its superior resolution and

ability to track non-stationary EEG dynamics and possibly non-linear interconnections. Notably, this paper introduces an approach to reveal the areas of interest at an EEG sensor level, which helps to better understand each brain area's contribution to the classification, of AD but this can also be applied to numerous other brain-related disorders.

Data availability statement

The data that support the findings of this study are available upon reasonable request from the authors.

Acknowledgment

The authors declare that they have no known competing financial interests or personal relationships that could have appeared to influence the work reported in this paper.

ORCID iDs

Jun Cao https://orcid.org/0000-0003-2121-7631
Yifan Zhao https://orcid.org/0000-0003-2383-5724

References

Abbasvandi Z and Nasrabadi A M 2019 A self-organized recurrent neural network for estimating the effective connectivity and its application to EEG data *Comput. Biol. Med.* **110** 93–107
Ahmadlou M, Adeli H and Adeli A 2012 Fuzzy synchronization likelihood-wavelet methodology for diagnosis of autism spectrum disorder *J. Neurosci. Methods* **211** 203–9
Allen E A 2018 EEG signatures of dynamic functional network connectivity *Brain Topogr.* **31** 101–16
Babiloni C *et al* 2013 Effects of acetylcholinesterase inhibitors and memantine on resting-state electroencephalographic rhythms in Alzheimer's disease patients *Clin. Neurophysiol.* **124** 837–50
Babiloni C, Lizio R, Marzano N, Capotosto P, Soricelli A, Triggiani A I, Cordone S, Gesualdo L and del Percio C 2016 Brain neural synchronization and functional coupling in Alzheimer's disease as revealed by resting state EEG rhythms *Int. J. Psychophysiol.* **103** 88–102
Barry R J and de Blasio F M 2017 EEG differences between eyes-closed and eyes-open resting remain in healthy ageing *Biol. Psychol.* **129** 293–304
Bell M A and Cuevas K 2012 Using EEG to study cognitive development: issues and practices *J. Cogn. Dev.* **13** 281–94
Benwell C S Y, Davila-Pérez P, Fried P J, Jones R N, Travison T G, Santarnecchi E, Pascual-Leone A and Shafi M M 2020 EEG spectral power abnormalities and their relationship with cognitive dysfunction in patients with Alzheimer's disease and type 2 diabetes *Neurobiol. Aging* **85** 83–95
Berrar D 2019 Cross-validation *Encyclopedia of Bioinformatics and Computational Biology: ABC of Bioinformatics* **1** 542–45
Blackburn D J *et al* 2018 A pilot study investigating a novel non-linear measure of eyes open versus eyes closed EEG synchronization in people with Alzheimer's disease and healthy controls *Brain Sci.* **8** 1–19
Blinowska K J, Rakowski F, Kaminski M, de Vico Fallani F, del Percio C, Lizio R and Babiloni C 2017 Functional and effective brain connectivity for discrimination between Alzheimer's patients and healthy individuals: a study on resting state EEG rhythms *Clin. Neurophysiol.* **128** 667–80
Cao J *et al* 2021a Using interictal seizure-free EEG data to recognise patients with epilepsy based on machine learning of brain functional connectivity *Biomed. Signal Process. Control* **67** 102554
Cao J, Zhao Y, Shan X, Wei H, Guo Y, Chen L, Erkoyuncu J A and Sarrigiannis P G 2021b Brain functional and effective connectivity based on electroencephalography recordings: a review *Hum. Brain Mapp.* **43** 1–20
Chen Y, Cai L, Wang R, Song Z, Deng B, Wang J and Yu H 2018 DCCA cross-correlation coefficients reveals the change of both synchronization and oscillation in EEG of Alzheimer disease patients *Physica* A **490** 171–84
Cohen M X 2017a Multivariate cross-frequency coupling via generalized eigendecomposition *eLife* **6** e21792
Cohen M X 2017b Where does EEG come from and what does it mean? *Trends Neurosci.* **40** 208–18
Cover T M and Thomas J A 2005 *Elements of Information Theory, Elements of Information Theory* (New York: Wiley)
delEtoile J and Adeli H 2017 Graph theory and brain connectivity in Alzheimer's disease *Neuroscientist* **23** 616–26
Dubois B *et al* 2007 Research criteria for the diagnosis of Alzheimer's disease: revising the NINCDS-ADRDA criteria *Lancet Neurol.* **6** 734–46
Durongbhan P *et al* 2019 A dementia classification framework using frequency and time-frequency features based on EEG signals *IEEE Trans. Neural Syst. Rehabil. Eng.* **27** 826–35
Engel A K, Gerloff C, Hilgetag C C and Nolte G 2013 Intrinsic coupling modes: multiscale interactions in ongoing brain activity *Neuron* **80** 867–86
Engels M M A *et al* 2015 Declining functional connectivity and changing hub locations in Alzheimer's disease: an EEG study *BMC Neurol.* **15** 1–8
Ferreri F *et al* 2016 Sensorimotor cortex excitability and connectivity in Alzheimer's disease: a TMS-EEG co-registration study *Hum. Brain Mapp.* **37** 2083–96
Fu K, Qu J, Chai Y and Dong Y 2014 Classification of seizure based on the time-frequency image of EEG signals using HHT and SVM *Biomed. Signal Process. Control* **13** 15–22
Grandy T H, Werkle-Bergner M, Chicherio C, Schmiedek F, Lövdén M and Lindenberger U 2013 Peak individual alpha frequency qualifies as a stable neurophysiological trait marker in healthy younger and older adults *Psychophysiol.* **50** 570–82
Gunawardena S R, Sarrigiannis P G, Blackburn D J and He F 2021 A kernel-based nonlinear manifold learning for EEG channel selection with application to Alzheimer's disease *bioRxiv Preprint* (https://doi.org/10.1101/2021.10.15.464451)
Handojoseno A M A, Shine J M, Nguyen T N, Tran Y, Lewis S J G and Nguyen H T 2013 Using EEG spatial correlation, cross frequency energy, and wavelet coefficients for the prediction of freezing of gait in Parkinson's disease patients *Proc. Annual Int. Conf. IEEE Engineering in Medicine and Biology Society (EMBS)* pp 4263–6
Hassan M *et al* 2017 Functional connectivity disruptions correlate with cognitive phenotypes in Parkinson's disease *Neuroimage Clin.* **14** 591–601
Huang N E, Shen Z, Long S R, Wu M C, Shih H H, Zheng Q, Yen N-C, Tung C C and Liu H H 1998 The empirical mode decomposition and the Hilbert spectrum for nonlinear and non-stationary time series analysis *Proc. R. Soc.* A **454** 903–95
Idaji M J, Zhang J, Stephani T, Nolte G, Müller K R, Villringer A and Nikulin V V 2022 Harmoni: a method for eliminating spurious interactions due to the harmonic components in neuronal data *Neuroimage* **252** 119053
Ieracitano C, Duun-Henriksen J, Mammone N, La Foresta F and Morabito F C 2017 Wavelet coherence-based clustering of EEG signals to estimate the brain connectivity in absence epileptic patients *Proc. Int. Joint Conf. Neural Networks* (*May 2017*) pp 1297–304
Jeong D H, Kim Y D, Song I U, Chung Y A and Jeong J 2016 Wavelet energy and wavelet coherence as EEG biomarkers

for the diagnosis of Parkinson's disease-related dementia and Alzheimer's disease *Entropy* **18** 8
Jones S R 2016 When brain rhythms aren't 'rhythmic': implication for their mechanisms and meaning *Curr. Opin. Neurobiol.* **40** 72–80
Kabbara A, El Falou W, Khalil M, Eid H and Hassan M 2017 A scalp-EEG network-based analysis of Alzheimer's disease patients at rest *Int. Conf. Advances Biomedical Engineering ICABME* (*October 2017*) pp 0–3
Keijzer H M, Tjepkema-Cloostermans M C, Klijn C J M, Blans M, van Putten M J A M and Hofmeijer J 2021 Dynamic functional connectivity of the EEG in relation to outcome of postanoxic coma *Clin. Neurophysiol.* **132** 157–64
Kent B A, Feldman H H and Nygaard H B 2021 Sleep and its regulation: an emerging pathogenic and treatment frontier in Alzheimer's disease *Prog. Neurobiol.* **197** 101902
Lachaux J-P, Rodriguez E, Martinerie J and Varela F 1999 Measuring phase synchrony in brain signals *Hum. Brain Mapp.* **8** 194–208
Lakshmi M R, Prasad T V and Prakash D V C 2014 Survey on EEG signal processing methods *Int. J. Adv. Res. Comput. Sci. Softw. Eng.* **4** 84–91
Law L S, Kim J H, Liew W Y H and Lee S K 2012 An approach based on wavelet packet decomposition and Hilbert–Huang transform (WPDHHT) for spindle bearings condition monitoring *Mech. Syst. Signal Process.* **33** 197–211
Li Y, Lei M, Cui W, Guo Y and Wei H L 2019 A parametric time frequency-conditional granger causality method using ultra-regularized orthogonal least squares and multiwavelets for dynamic connectivity analysis in EEGs *IEEE Trans. Biomed. Eng.* **66** 3509–25
Liu X *et al* 2016 Multiple characteristics analysis of Alzheimer's electroencephalogram by power spectral density and Lempel–Ziv complexity *Cogn. Neurodyn.* **10** 121–33
Lotte F, Bougrain L, Cichocki A, Clerc M, Congedo M, Rakotomamonjy A and Yger F 2018 A review of classification algorithms for EEG-based brain-computer interfaces: a 10 year update *J. Neural Eng.* **15** 031005
Mazaheri A and Jensen O 2008 Asymmetric amplitude modulations of brain oscillations generate slow evoked responses *J. Neurosci.* **28** 7781–7
McBride J, Zhao X, Munro N, Jicha G, Smith C and Jiang Y 2015 Discrimination of mild cognitive impairment and Alzheimer's disease using transfer entropy measures of scalp EEG *J. Healthc. Eng.* **6** 55–70
Melia U, Guaita M, Vallverdú M, Embid C, Vilaseca I, Salamero M and Santamaria J 2015 Mutual information measures applied to EEG signals for sleepiness characterization *Med. Eng. Phys.* **37** 297–308
Mheich A, Hassan M, Khalil M, Berrou C and Wendling F 2015 A new algorithm for spatiotemporal analysis of brain functional connectivity *J. Neurosci. Methods* **242** 77–81
Miraglia F, Vecchio F, Bramanti P and Rossini P M 2016 EEG characteristics in 'eyes-open' versus 'eyes-closed' conditions: small-world network architecture in healthy aging and age-related brain degeneration *Clin. Neurophysiol.* **127** 1261–8
Moca V V, Bârzan H, Nagy-Dăbâcan A and Mureșan R C 2021 Time-frequency super-resolution with superlets *Nat. Commun.* **12** 1–18
Mousavi A A, Zhang C, Masri S F and Gholipour G 2020 Structural damage localization and quantification based on a CEEMDAN Hilbert transform neural network approach: a model steel truss bridge case study *Sensors* **20** 1271
Nimmy J T, Subha D P and Menon R N 2019 Mutual information analysis on MCI-AD EEG signal during resting and task conditions *IEEE Region 10 Annual Int. Conf. Proc./TENCON* (*October 2019*) pp 2295–9
Nir R R, Sinai A, Raz E, Sprecher E and Yarnitsky D 2010 Pain assessment by continuous EEG: association between subjective perception of tonic pain and peak frequency of alpha oscillations during stimulation and at rest *Brain Res.* **1344** 77–86
Peng Z K, Tse P W and Chu F L 2005 A comparison study of improved Hilbert–Huang transform and wavelet transform: application to fault diagnosis for rolling bearing *Mech. Syst. Signal Process.* **19** 974–88
Pfurtscheller G and Andrew C 1999 Event-related changes of band power and coherence: methodology and interpretation *J. Clin. Neurophysiol.* **16** 512
Pijnenburg Y A L, Vd Made Y, van Walsum A V C, Knol D L, Scheltens P and Stam C J 2004 EEG synchronization likelihood in mild cognitive impairment and Alzheimer's disease during a working memory task *Clin. Neurophysiol.* **115** 1332–9
Poil S S, de Haan W, van der Flier W M, Mansvelder H D, Scheltens P and Linkenkaer-Hansen K 2013 Integrative EEG biomarkers predict progression to Alzheimer's disease at the MCI stage *Front. Aging Neurosci.* **5** 1–12
Posthuma D, Neale M C, Boomsma D I and de Geus E J C 2001 Are smarter brains running faster? Heritability of alpha peak frequency, IQ, and their interrelation *Behav. Genet.* **31** 567–79
Qiao J, Lv Y, Cao C, Wang Z and Li A 2018 Multivariate deep learning classification of Alzheimer's disease based on hierarchical partner matching independent component analysis *Front. Aging Neurosci.* **10** 1–12
Sadaghiani S and Kleinschmidt A 2016 Brain networks and α-oscillations: structural and functional foundations of cognitive control *Trends Cogn. Sci.* **20** 805–17
Sakkalis V 2011 Review of advanced techniques for the estimation of brain connectivity measured with EEG/MEG *Comput. Biol. Med.* **41** 1110–7
Sankari Z and Adeli H 2011 Probabilistic neural networks for diagnosis of Alzheimer's disease using conventional and wavelet coherence *J. Neurosci. Methods* **197** 165–70
Sankari Z, Adeli H and Adeli A 2011 Intrahemispheric, interhemispheric, and distal EEG coherence in Alzheimer's disease *Clin. Neurophysiol.* **122** 897–906
Sankari Z, Adeli H and Adeli A 2012 Wavelet coherence model for diagnosis of Alzheimer disease *Clin. EEG Neurosci.* **43** 268–78
Scally B, Burke M R, Bunce D and Delvenne J F 2018 Resting-state EEG power and connectivity are associated with alpha peak frequency slowing in healthy aging *Neurobiol. Aging* **71** 149–55
Schmidt M T *et al* 2013 Index of alpha/theta ratio of the electroencephalogram: a new marker for Alzheimer's disease *Front. Aging Neurosci.* **5** 1–6
Shan X, Huo S, Cao J, Yang L, Zou J, Chen L and Li Z 2021 Tracking non-stationary association of two electroencephalography signals using a revised Hilbert–Huang transformation *IEEE Trans. Neural Syst. Rehabil. Eng.* **29** 841–51
Smit C M, Wright M J, Hansell N K, Geffen G M and Martin N G 2006 Genetic variation of individual alpha frequency (IAF) and alpha power in a large adolescent twin sample *Int. J. Psychophysiol.* **61** 235–43
Su R, Li X, Li Z, Han Y, Cui W, Xie P and Liu Y 2021 Constructing biomarker for early diagnosis of aMCI based on combination of multiscale fuzzy entropy and functional brain connectivity *Biomed. Signal Process. Control* **70** 103000
Tafreshi T F, Daliri M R and Ghodousi M 2019 Functional and effective connectivity based features of EEG signals for object recognition *Cogn. Neurodyn.* **13** 555–66
Torres M E, Colominas M A, Schlotthauer G and Flandrin P 2011 A complete ensemble empirical mode decomposition with adaptive noise *2011 IEEE Int. Conf. Acoustics Speech Signal Processing (ICASSP)* pp 4144–7
van der Zande J J, Gouw A A, van Steenoven I, Scheltens P, Stam C J and Lemstra A W 2018 EEG characteristics of dementia with Lewy bodies, Alzheimer's disease and mixed pathology *Front. Aging Neurosci.* **10** 1–10

van Mierlo P, Papadopoulou M, Carrette E, Boon P, Vandenberghe S, Vonck K and Marinazzo D 2014 Functional brain connectivity from EEG in epilepsy: seizure prediction and epileptogenic focus localization *Prog. Neurobiol.* **121** 19–35

Varotto G, Fazio P, Rossi Sebastiano D, Duran D, D'Incerti L, Parati E, Sattin D, Leonardi M, Franceschetti S and Panzica F 2014 Altered resting state effective connectivity in long-standing vegetative state patients: an EEG study *Clin. Neurophysiol.* **125** 63–68

Vecchio F, Miraglia F, Alù F, Menna M, Judica E, Cotelli M and Rossini P M 2020 Classification of Alzheimer's disease with respect to physiological aging with innovative EEG biomarkers in a machine learning implementation *J. Alzheimer's Dis.* **75** 1253–61

Vecchio F, Miraglia F, Piludu F, Granata G, Romanello R, Caulo M, Onofrj V, Bramanti P, Colosimo C and Rossini P M 2017 'Small world' architecture in brain connectivity and hippocampal volume in Alzheimer's disease: a study via graph theory from EEG data *Brain Imaging Behav.* **11** 473–85

Wang R, Wang J, Li H and Chen Y 2015a Power spectral density and high order bispectral analysis of Alzheimer's EEG *Proc. 2015 27th Chinese Control Decision Conf. CCDC 2015* pp 1822–6

Wang R, Wang J, Yu H, Wei X, Yang C and Deng B 2015b Power spectral density and coherence analysis of Alzheimer's EEG *Cogn. Neurodyn.* **9** 291–304

Wang R, Yang Z, Wang J and Shi L 2017 Power spectral density and Lempel-Ziv complexity analysis of EEG in Alzheimer's disease *Chinese Control Conf. (CCC)* pp 5549–54

Wells W 1996 Multi-modal volume registration by maximization of mutual information *Med. Image Anal.* **1** 35–51

Wu Z and Huang N E 2009 Ensemble empirical mode decomposition: a noise-assisted data analysis method *Adv. Adapt. Data Anal.* **1** 1–41

Yao W and Wang J 2017 Multi-scale symbolic transfer entropy analysis of EEG *Physica* A **484** 276–81

Yu H, Lei X, Song Z, Wang J, Wei X and Yu B 2018 Functional brain connectivity in Alzheimer's disease: an EEG study based on permutation disalignment index *Physica* A **506** 1093–103

Zhao Y *et al* 2020 Imaging of nonlinear and dynamic functional brain connectivity based on EEG recordings with the application on the diagnosis of Alzheimer's disease *IEEE Trans. Med. Imaging* **39** 1571–81